bioRxiv preprint doi: https://doi.org/10.1101/2023.12.17.572059; this version posted December 17, 2023. The copyright holder for this preprint (which was not certified by peer review) is the author/funder, who has granted bioRxiv a license to display the preprint in perpetuity. It is made available under a CC-BY-NC-ND 4.0 International license.

An ovine model for investigation of the microenvironment of the male mammary gland

Benjamin P. Davies[1], Rachael C. Crew[2,3], Anna L. K. Cochrane[2], Katie Davies[2], Andre Figueiredo Baptista[1], Sonja Jeckel[4], Ian McCrone[1], Youguo Niu[2], Benjamin W. Strugnell[5], Katie Waine[5,6], Abigail L. Fowden[2], Clare E. Bryant[1], John W. Wills[1], Dino A. Giussani[2], Katherine Hughes[1*]

1. Department of Veterinary Medicine, University of Cambridge, Cambridge, UK.
2. Department of Physiology, Development and Neuroscience, University of Cambridge, Cambridge, UK.
3. Department of Obstetrics and Gynaecology, University of Cambridge, UK.
4. Farm Animal Pathology and Diagnostics, The Royal Veterinary College, Hatfield, UK.
5. Farm Post Mortems Ltd, Durham, UK.
6. Current address: Faculty of Veterinary Medicine, University of Calgary, Calgary, AB T3R 1J3, Canada.

*Correspondence: Katherine Hughes, Department of Veterinary Medicine, University of Cambridge, Madingley Road, Cambridge, CB3 0ES, UK. Email kh387@cam.ac.uk

Running page heading

Microenvironment of the male sheep mammary gland

bioRxiv preprint doi: https://doi.org/10.1101/2023.12.17.572059; this version posted December 17, 2023. The copyright holder for this preprint (which was not certified by peer review) is the author/funder, who has granted bioRxiv a license to display the preprint in perpetuity. It is made available under a CC-BY-NC-ND 4.0 International license.

Abstract

The specific biology of the male breast remains relatively unexplored in spite of the increasing global prevalence of male breast cancer. Delineation of the microenvironment of the male breast is restricted by the low availability of human samples and a lack of characterisation of appropriate animal models. Unlike the mouse, the male ovine gland persists postnatally. We suggest that the male ovine mammary gland constitutes a promising adjunctive model for the male human breast. In this study we evaluate the male ovine mammary gland microenvironment, comparing intact and neutered males. Assessment of the glandular histo-anatomy highlights the resemblance of the male gland to that of the neonatal female sheep and confirms the presence of rudimentary terminal duct lobular units. Irrespective of neutered status, cell proliferation in epithelial and stromal compartments is low in males, and cell proliferation in epithelial cells and in the intralobular stroma is significantly lower than in pubertal female sheep. Between 42% and 72% of the luminal mammary epithelial cells in the male gland express the androgen receptor, and expression is significantly reduced by neutering. Luminal epithelial cells within the intact and neutered male gland also express oestrogen receptor alpha, but minimal progesterone receptor expression is observed. The distrubution of mammary leukocytes within the ducts and stroma is similar in the female mammary gland of sheep and other species. Both macrophages and T lymphocytes are intercalated in the epithelial bilayer and are more abundant in the intralobular stroma than the interlobular stroma, suggesting that they may have a protective immunological function within the vestigial glandular tissue of the male sheep. Mast cells are also observed within the stroma. These cells cluster nearer the glandular tissue and are frequently located adjacent to blood vessels. The abundance of mast cells is significantly higher in intact males compared to neutered males, suggesting that hormone signalling may impact mast cell recruitment. In this study, we demonstrate the utility of the male ovine

bioRxiv preprint doi: https://doi.org/10.1101/2023.12.17.572059; this version posted December 17, 2023. The copyright holder for this preprint (which was not certified by peer review) is the author/funder, who has granted bioRxiv a license to display the preprint in perpetuity. It is made available under a CC-BY-NC-ND 4.0 International license.

mammary gland as a model for furthering our knowledge of postnatal male mammary biology.

Keywords

Male; mammary gland; microenvironment; model; sheep; udder

bioRxiv preprint doi: https://doi.org/10.1101/2023.12.17.572059; this version posted December 17, 2023. The copyright holder for this preprint (which was not certified by peer review) is the author/funder, who has granted bioRxiv a license to display the preprint in perpetuity. It is made available under a CC-BY-NC-ND 4.0 International license.

Introduction

The mammary gland nourishes and supports the development of offspring. Whilst they are intrinsically linked with female individuals, mammary glands persist in the majority of male mammals, although with notable exceptions including mice, horses and marsupials (Cardiff et al., 2018; Hughes, 2021a; Renfree et al., 1990).

Early fetal development of the male mammary gland is typically consistent with that of the female, irrespective of species (Hassiotou and Geddes, 2013; Jenkinson, 2003; Pokharel et al., 2018). Between embryonic day 11 and 13 of fetal mouse development, mammary placodes are established from ectoderm thickening on bilateral milk lines (Macias and Hinck, 2012; Stewart et al., 2019). The mammary placodes then invaginate into the mesenchyme layer, forming mammary buds (Paine and Lewis, 2017). Sexual dimorphism of the mouse mammary gland is established at embryonic day 14 (Richert et al., 2000; Stewart et al., 2019). In male mice, androgen is produced from the developing testes which causes condensation of the mesenchyme within the developing mammary gland (Dürnberger and Kratochwil, 1980; Richert et al., 2000; Vandenberg et al., 2013). This results in the morphological distortion of the mammary epithelium detaching the gland from the overlying epidermis (Drews and Drews, 1977; Richert et al., 2000; Stewart et al., 2019). The gland thereafter regresses and at birth comprises minimal vestigial glandular tissue that lacks nipples (Cardiff et al., 2018; Pokharel et al., 2018; Szabo and Vandenberg, 2021). In some genetically modified mouse strains, glandular tissue can persist after birth (Pokharel et al., 2018; Szabo and Vandenberg, 2021) but may still lack key developmental structures required for mammary gland expansion such as terminal end buds (Kolla et al., 2017).

bioRxiv preprint doi: https://doi.org/10.1101/2023.12.17.572059; this version posted December 17, 2023. The copyright holder for this preprint (which was not certified by peer review) is the author/funder, who has granted bioRxiv a license to display the preprint in perpetuity. It is made available under a CC-BY-NC-ND 4.0 International license.

By contrast, human prepubescent breast development is consistent between the sexes until the influence of androgen at puberty limits both ductal and stromal expansion of male breast tissue (Hassiotou and Geddes, 2013; Jesinger, 2014). The male breast comprises a small arborising ductal tree, apparently largely without well-developed lobules, embedded in an adipose-rich stroma (Fox et al., 2022).

The male breast has the potential to develop similar pathologies to that of females but at a lower incidence (Chatterji et al., 2023; Iuanow et al., 2011). However, there has been less focus on the specific biology of the male breast. Prevalence of male breast cancer is increasing globally (Fox et al., 2022) and the risk of death is significantly higher than comparable female breast cancers (Liu et al., 2018). Male breast neoplasms also have different biology compared to breast neoplasms arising in women (Chatterji et al., 2023). Research focussed specifically on the male breast is currently limited by both the low availability of human samples and the lack of characterisation of appropriate animal models in which the complete male mammary structure persists postnatally.

Sheep are commonly used to model human fetal development (Morrison et al., 2018) and we and others have noted anatomical similarities in mammary terminal duct lobular unit (TDLU) structure and stromal composition between the sheep mammary gland and the female breast (Hovey et al., 1999; Hughes, 2021b; Hughes and Watson, 2018; Nagy et al., 2021; Rowson et al., 2012). Male and female ovine fetuses exhibit parallel mammary developmental, with the gland and teat cistern present in both sexes around fetal day 80 (Jenkinson, 2003). However, there has been little examination of the male ovine mammary gland postnatally. We suggest that the mammary gland of the male sheep may constitute a promising model of the male

bioRxiv preprint doi: https://doi.org/10.1101/2023.12.17.572059; this version posted December 17, 2023. The copyright holder for this preprint (which was not certified by peer review) is the author/funder, who has granted bioRxiv a license to display the preprint in perpetuity. It is made available under a CC-BY-NC-ND 4.0 International license.

105 human breast. Consequently, in this study we evaluate the mammary microenvironment in the
106 male sheep, comparing intact and neutered males to highlight how male specific sex
107 hormones may affect the mammary microenvironment.

108

109 **Materials and Methods**

110 *Animals*

111 Ovine mammary tissue was obtained from both male and female sheep that were submitted to
112 the diagnostic veterinary anatomic pathology services of either the Department of Veterinary
113 Medicine, University of Cambridge or to the Royal Veterinary College. Mammary tissue was
114 also collected during the post mortem examination of Welsh mountain sheep, euthanised for
115 research purposes under the Animals (Scientific Procedures) Act 1986. The Ethics and
116 Welfare Committee of the Department of Veterinary Medicine, University of Cambridge,
117 approved the study plan to use post mortem tissue in this project (references: CR223 and
118 CR625). The nonregulated scientific use of post mortem mammary tissue collected from
119 research animals was approved by the Named Veterinary Surgeon of the University of
120 Cambridge. Any tissue containing evidence of mammary pathology was excluded from the
121 study.

122

123 Male sheep used in this study ranged from 3 days old to 3 years old, but only animals older
124 than 4 months were included in quantification analysis. Pubertal female sheep were aged
125 from 4 months to 11 months. Mature female sheep were all older than two years and were not
126 expected to be oestrus cycling based on the time of year of the post mortem examination
127 (sheep are seasonal breeders). The sheep used were from a variety of breeds (Supplementary
128 Table 1).

bioRxiv preprint doi: https://doi.org/10.1101/2023.12.17.572059; this version posted December 17, 2023. The copyright holder for this preprint (which was not certified by peer review) is the author/funder, who has granted bioRxiv a license to display the preprint in perpetuity. It is made available under a CC-BY-NC-ND 4.0 International license.

Tissue processing

Mammary tissue was fixed in 10% neutral-buffered formalin for approximately one week. The entire male mammary gland and samples of female mammary parenchyma were then trimmed, processed using a routine histology protocol and embedded in paraffin. Sections were cut at 5 µm and mounted on coated glass slides (TOMO®) or stained with haematoxylin and eosin to check for microscopic pathology prior to inclusion in the study.

Dual immunohistochemistry and immunofluorescence

Formalin fixed paraffin embedded (FFPE) tissue was subjected to antigen retrieval using a PT link module and high pH antigen retrieval solution (both Dako Pathology/Agilent Technologies, Stockport, UK). For dual immunohistochemistry, an ImmPRESS® Duet Double Staining Polymer Kit (Vector Laboratories) was used. Primary antibodies were added at the appropriate concentration (Supplementary Table 2) and incubated overnight at 4°C. Negative controls received isotype- and species-matched immunoglobulins. Counterstaining was achieved by incubating in Mayer's Haematoxylin for 4 minutes. Slides were dehydrated in an ethanol and xylene series and Pertex® Mounting Medium was added dropwise. ClariTex Coverslips (24 x 50mm) were then applied.

For immunofluorescence, slides were first incubated with 10% normal goat serum for 1 hour at room temperature. Primary antibodies were added at the appropriate concentration (Supplementary Table 2) and incubated overnight at 4°C. Slides were then incubated in darkness with secondary antibodies (Supplementary Table

bioRxiv preprint doi: https://doi.org/10.1101/2023.12.17.572059; this version posted December 17, 2023. The copyright holder for this preprint (which was not certified by peer review) is the author/funder, who has granted bioRxiv a license to display the preprint in perpetuity. It is made available under a CC-BY-NC-ND 4.0 International license.

2) for 1 hour at room temperature. Negative controls received isotype- and species-matched immunoglobulins. Nuclei staining was performed by incubating with DAPI (10.9 µM) (SigmaAldrich/Merck Life Science UK Limited, Gillingham, UK) for 5 minutes. Slides were cover-slipped using Vectashield® VibranceTM Antifade mounting medium (catalogue H-1700; Vector laboratories, Peterborough, UK) and imaged using a Leica TCS SP8 confocal microscope.

Clear, unobstructed brain imaging cocktails (CUBIC)

Mammary tissue was dissected and fixed in 10% neutral-buffered formalin for 6 to 26 hours. The gland was trimmed into smaller samples, approximately 15 x 15 x 5 mm. These samples were optically cleared using the CUBIC protocol (Lloyd-Lewis et al., 2016; Susaki et al., 2014) with the modifications outlined below. Tissue was incubated in CUBIC reagent 1A for 4 days on a shaker at 37°C. The solution was replaced daily. Samples were then incubated overnight, on at shaker at 4°C, with a blocking solution containing normal goat serum [10% (volume per volume)] and Triton X-100 [0.5% (weight per volume)] in phosphate-buffered saline (PBS). Primary antibodies, diluted in blocking solution, were applied at appropriate concentrations (Supplementary Table 2) and samples were incubated for 4 days on a shaker at 4 °C. Tissue samples were subsequently thoroughly washed in PBS and secondary antibodies (Supplementary Table 2), also diluted in blocking solution, were then applied. Samples were incubated in darkness on a shaker at 4 °C. Negative controls received isotype- and species-matched immunoglobulins. After further washing in PBS containing Triton X-100 (0.1% (weight per weight)), nuclei staining was performed by incubating in DAPI (10.9 µM) (SigmaAldrich/Merck Life Science UK Limited, Gillingham, UK) at room temperature for at least 1 hour. After further washing, CUBIC reagent 2 was applied and incubated in darkness

bioRxiv preprint doi: https://doi.org/10.1101/2023.12.17.572059; this version posted December 17, 2023. The copyright holder for this preprint (which was not certified by peer review) is the author/funder, who has granted bioRxiv a license to display the preprint in perpetuity. It is made available under a CC-BY-NC-ND 4.0 International license.

for 4 days on shaker at 37 °C. Tissue samples were imaged in Ibidi 35 mm glass bottom dishes (catalogue 81218-200; ibidi GmbH, Gräfelfing, Germany) using a Leica TCS SP8 confocal microscope.

Slide scanning

Slides subjected to immunohistochemical staining were scanned at 40× magnification using a NanoZoomer 2.0RS, C10730, (Hamamatsu Photonics, Hamamatsu City, Japan). Scanned sections were analysed with viewing software (NDP.view2, Hamamatsu Photonics).

Sampling for cell proliferation and immune cell abundance

Slide scans were analysed with NDP.view2 viewing software. Depending on the tissue area available for analysis, three to eight count boxes (400 × 230 µm) were randomly placed on each slide at 1.25x magnification. Boxes containing artefacts from slide cutting or scanning were repositioned.

Quantification of epithelial and stromal proliferation

Instances of myoepithelial and luminal cell proliferation, and proliferation of any cells located within the interlobular and intralobular stroma, as denoted by positive nuclear Ki67 staining, were manually counted. The total count for all sample boxes on the slide was calculated. This total count was then normalised to the total sampled area (mm^2) of glandular tissue, interlobular or intralobular stroma, calculated by tracing around the area using the NDP.view2 freehand annotation tool. The protocol was repeated for all individuals within each experimental group and the mean was derived.

bioRxiv preprint doi: https://doi.org/10.1101/2023.12.17.572059; this version posted December 17, 2023. The copyright holder for this preprint (which was not certified by peer review) is the author/funder, who has granted bioRxiv a license to display the preprint in perpetuity. It is made available under a CC-BY-NC-ND 4.0 International license.

Manual quantification of hormone receptor expression

A Leica TCS SP8 confocal microscope was utilised to produce x400 magnification tile scans of immunofluorescence slides. Tile scans were analysed using Fiji (Schindelin et al., 2012), and, depending on the size of the tissue, three to eight count boxes (each measuring 400 × 230 µm) were randomly placed on each slide at low magnification. Hormone receptor positive luminal epithelial cell nuclei were manually counted and the total count for all sample boxes on the slide was calculated. This count was expressed as a percentage of the total number of luminal epithelial cell nuclei within all sample count boxes. The protocol was repeated for all individuals within each experimental group and the mean percentage of hormone receptor positive luminal cell nuclei for each group was calculated.

Epithelial and Stromal Macrophage and T lymphocyte abundance

Using NDP.view2, the number of epithelial-associated IBA1 positive-macrophages and CD3-positive T lymphocytes were counted. Cells were considered epithelial-associated if >50% of their cytoplasmic perimeter contacted the basement membrane. The total number of epithelial-associated macrophages and T lymphocytes in all count boxes was calculated for each individual, together with the total number of epithelial cells, and the epithelial-associated immune cell count was expressed per 100 luminal epithelial cells. Stromal macrophages and T lymphocytes were considered to be interlobular and intralobular respectively when >50% of their cytoplasmic perimeter was within the respective type of stroma. The total number of macrophages and T lymphocytes for each stroma type was calculated. This count was normalised to the total sampled area (mm^2) of interlobular or

bioRxiv preprint doi: https://doi.org/10.1101/2023.12.17.572059; this version posted December 17, 2023. The copyright holder for this preprint (which was not certified by peer review) is the author/funder, who has granted bioRxiv a license to display the preprint in perpetuity. It is made available under a CC-BY-NC-ND 4.0 International license.

intralobular stroma, determined using the NDP.view2 freehand annotation tool. The protocol was repeated for all individuals within each experimental group and the mean was derived.

Statistical analysis

To assess statistical significance in comparisons between cell proliferation and comparisons between hormone receptor expression, a Kruskal-Wallis test was conducted. Statistical significance in the differences in immune cell abundance between intact and neutered males were assessed using a Mann-Whitney U test. To assess statistical significance in the differences in immune cell abundance between intra- and interlobular stroma, a Wilcoxon signed-rank test was performed. All data were collected using Microsoft Excel and were analysed using R studio (RStudio: Integrated Development for R. RStudio, PBC, Boston, MA URL http://www.rstudio.com/). All data are presented as mean values + the standard deviation.

Results and Discussion

The gross and histo-anatomy of the male sheep mammary gland resembles that of the neonatal female.

In total, thirty-three sheep were analysed in the study (Suppl. Table 1) Nineteen of these sheep were male, comprising eight intact males and eleven neutered males. These male sheep ranged between three days old to three years old, but only male sheep older than four months were included in analyses involving quantification. These male sheep were of several different breeds, including four Cheviot cross males, three Welsh mountain males, three Texel cross males and one of each of Jacob cross, New Zealand Romney, Suffolk, Mule, Mule cross

bioRxiv preprint doi: https://doi.org/10.1101/2023.12.17.572059; this version posted December 17, 2023. The copyright holder for this preprint (which was not certified by peer review) is the author/funder, who has granted bioRxiv a license to display the preprint in perpetuity. It is made available under a CC-BY-NC-ND 4.0 International license.

and Shetland. For three male sheep no breed information was available. Male sheep were compared to a group of seven pubertal female sheep and seven mature female ewes. Pubertal females ranged from four to eleven months in age. These ewes were of three different breeds comprising five Welsh mountain ewes and one each of Texel cross and Beltex. Mature females were all older than two years and all seven were Welsh mountain ewes.

To investigate the possibility that the mammary gland of the male sheep is a useful adjunct model for the male breast, we initially characterised the gross and histo-anatomy of the gland. The male sheep mammary gland is located in the sub-epithelial tissues below the teat (Fig. 1 a) and is composed of branching ducts that terminate in terminal duct lobular units (TDLUs) (Fig. 1 b-e). The walls of the ducts comprise a bilayer of luminal epithelial cells and basal myoepithelial cells (Fig. 1 b). Both intra- and interlobular mammary stroma surrounds the ductal system (Fig. 1 c) and, like that of the female ruminant, expresses smooth muscle actin (Nagy et al., 2021; Safayi et al., 2012). Overall the structure of the male gland is very similar to that of the neonatal female sheep (Hughes, 2021b; Nagy et al., 2021) and contrasts the minimal vestigial glandular tissue present in the postnatal male mouse mammary gland (Cardiff et al., 2018; Pokharel et al., 2018; Stewart et al., 2019; Szabo and Vandenberg, 2021).

The male ovine mammary gland exhibits minimal cell proliferation, irrespective of neutered status.

Given that the female mammary gland undergoes dynamic changes in cell proliferation throughout its postnatal development cycle (Inman et al., 2015) we wished to assess the proliferation dynamics of different cellular compartments within the male gland, comparing

bioRxiv preprint doi: https://doi.org/10.1101/2023.12.17.572059; this version posted December 17, 2023. The copyright holder for this preprint (which was not certified by peer review) is the author/funder, who has granted bioRxiv a license to display the preprint in perpetuity. It is made available under a CC-BY-NC-ND 4.0 International license.

intact and neutered male animals with pubertal females and mature females. Proliferation in both epithelial and stromal compartments is similarly low in male sheep irrespective of neuter status. Proliferation in luminal epithelial cells, myoepithelial cells and cells present in the intralobular stroma, is significantly higher in pubertal females when compared to both intact and neutered males (Fig 2 e-g).

Neutering decreases mammary androgen receptor expression in sheep.

In our study population, between 42% and 72% of luminal mammary epithelial cells in intact male sheep express androgen receptor (AR) and expression is abrogated by neutering (Fig. 3). Previously studies have illustrated that androgen receptor activation limits the expansion of glandular tissue within the female mammary gland. Transgenic mouse models in which the production or action of AR was ablated, exhibited increased cell proliferation, ductal branching and number of terminal end buds (Gao et al., 2014; Simanainen et al., 2012). In humans, AR functions to limit the growth of breast tissue in both prepubescent boys and girls (Dimitrakakis and Bondy, 2009), and our data in the sheep are consistent with this observation.

Oestrogen receptor alpha (ER alpha) expression has previously been highlighted in epithelial cells within the TDLUs of prepubertal sheep (Colitti and Parillo, 2013) and is similarly observed in both male and female groups in our study (Fig. 3e- 3h). Our analysis indicates that intact males have a higher percentage of luminal epithelial cells exhibiting ER alpha expression than mature females (Fig. 3n), potentially reflecting a variable composition of luminal epithelial sub-groups in the male gland compared to the female. Understanding the balance between AR and ER alpha expression in the male mammary gland is important

bioRxiv preprint doi: https://doi.org/10.1101/2023.12.17.572059; this version posted December 17, 2023. The copyright holder for this preprint (which was not certified by peer review) is the author/funder, who has granted bioRxiv a license to display the preprint in perpetuity. It is made available under a CC-BY-NC-ND 4.0 International license.

because the vast majority of male breast cancer is ER positive (Cardoso et al., 2018; Chatterji et al., 2023).

Mean progesterone receptor expression is higher in pubertal females than neutered males (Fig. 3o). Progesterone receptor expression has been previously reported in the alveolar cells of the female ovine mammary gland during lactation (Colitti and Parillo, 2013) and prior research, using hormone treated murine mammary glands, indicates that progesterone receptor signalling promotes ductal branching during puberty (Atwood et al., 2000). Progesterone receptor signalling has also been shown to promote cell proliferation in multiple mammary cell types during puberty and pregnancy (Atwood et al., 2000; Brisken et al., 1998; Hilton et al., 2015). The low expression of progesterone receptor in neutered males and low but variable levels of progesterone receptor expression in intact males are consistent with the relatively limited tissue area occupied by the male gland and the lack of cell proliferation we observe within the male mammary gland (Fig. 2e-2h).

Macrophages and T lymphocytes are intercalated in the epithelial bilayer and cluster nearer ductal structures in the male ovine mammary gland.

In both intact and neutered male sheep, IBA-1 positive macrophages are intercalated in the epithelial bilayer and are present in the intra- and interlobular mammary stroma. There are abundant macrophages surrounding the TDLUs and many are intimately associated with the epithelium (Fig. 4). The localisation of mammary macrophages in the male sheep is overall consistent with previous characterisation of the female neonatal and pubertal ovine mammary gland, with the exception that the macrophages within the male gland do not appear to exhibit the periodicity previously noted in females (Nagy et al., 2021). The intraepithelial

bioRxiv preprint doi: https://doi.org/10.1101/2023.12.17.572059; this version posted December 17, 2023. The copyright holder for this preprint (which was not certified by peer review) is the author/funder, who has granted bioRxiv a license to display the preprint in perpetuity. It is made available under a CC-BY-NC-ND 4.0 International license.

317 macrophages of the male gland may be similar to the ductal macrophages reported in the
318 mouse mammary gland (Dawson et al., 2020). These ductal macrophages have phenotypes
319 and gene expression patterns distinct from stromal macrophages, reflecting an immune
320 surveillance function (Dawson et al., 2020). The macrophages within the male ovine gland
321 could have a similar role, but their precise phenotype and function requires further
322 elucidation. In female mice, macrophage abundance also is affected by oestrogen and
323 progesterone, during oestrus cycling (Chua et al., 2010; Hodson et al., 2013; Tower et al.,
324 2022) and macrophages are receptive to androgen signalling (Liva and Voskuhl, 2001).
325 However, our data suggest that male ovine mammary gland macrophage abundance is
326 unaffected by neutered status (Suppl. Fig 1), an observation warranting further future
327 investigation.

328

329 In both intact and neutered males, the abundance of macrophages is significantly higher in
330 the intralobular stroma, directly surrounding the glandular tissue, compared to the more
331 distant interlobular stroma (Fig. 4). This is consistent with previous examination of the
332 female bovine mammary gland (Beaudry et al., 2016).

333

334 Similar to epithelial-associated macrophages, CD3 positive T lymphocytes are intercalated in
335 the epithelial bilayer and are present in the intra- and interlobular mammary stroma. In
336 contrast, there are few CD20-positive B lymphocytes (Fig. 5). Comparisons between intact
337 and neutered males highlight that there is no significant difference in abundance of T
338 lymphocytes associated with the epithelium or in the intra- or interlobular stroma (Suppl. Fig.
339 2). In neutered males there are more T lymphocytes in the intralobular stroma than in the
340 interlobular stroma (Fig. 5). The clustering of both macrophages and T lymphocytes within

bioRxiv preprint doi: https://doi.org/10.1101/2023.12.17.572059; this version posted December 17, 2023. The copyright holder for this preprint (which was not certified by peer review) is the author/funder, who has granted bioRxiv a license to display the preprint in perpetuity. It is made available under a CC-BY-NC-ND 4.0 International license.

and near the male mammary ductal structures may imply that they have an active immunological function with the male ovine vestigial glandular tissue, which has a potential portal for ingress of pathogens from the exterior through the teat.

Mast cells cluster nearer ductal structures in the male ovine mammary gland and their abundance is significantly higher in intact males.

Mast cells have been previously identified in the mammary gland of the mouse (Hughes et al., 2012; Lilla and Werb, 2010), rat (Ramirez et al., 2012) and cow (Beaudry et al., 2016). Typically, histological identification of mast cells is carried out using toluidine blue staining to highlight the cells' metachromatic staining granules. We and others have used toluidine blue to identify mast cells in the mammary gland of laboratory rodents (Hughes et al., 2012; Lilla and Werb, 2010; Ramirez et al., 2012). However, toluidine blue staining does not positively stain mast cells in the ovine mammary gland, potentially due to differences in granule composition (Suppl. Fig. 3). Consequently, we have stained for c-Kit, a transmembrane tyrosine kinase receptor (Ribatti, 2018), that has been previously used to identify mast cells in human tissues (Lammie et al., 1994). Mast cells are present in the mammary stroma in both intact and neutered male glands and are present in close proximity to blood vessels (Fig. 6). This localisation is consistent with previous descriptions of mast cells in the female mouse mammary gland (Lilla and Werb, 2010).

The abundance of mast cells in the intra- and interlobular stroma is significantly higher in intact males compared to neutered males (Fig. 6d - e), suggesting that steroid hormone signalling may impact mast cell recruitment. A prior study highlighted that mast cells within the human skin express androgen receptors, but mast cell degranulation remained unchanged

bioRxiv preprint doi: https://doi.org/10.1101/2023.12.17.572059; this version posted December 17, 2023. The copyright holder for this preprint (which was not certified by peer review) is the author/funder, who has granted bioRxiv a license to display the preprint in perpetuity. It is made available under a CC-BY-NC-ND 4.0 International license.

upon the administration of a testosterone treatment (Chen et al., 2010). However, authors did not comment how testosterone treatment may have affected mast cell abundance. There is also some evidence that oestrogen could affect mast cell recruitment in the female bovine mammary gland, where researchers identified a trend in which that mast cell number increases upon the exogenous oestrogen treatment (Beaudry et al., 2016). Elucidating how specific hormone receptor signalling may affect mast cell recruitment within the male ovine gland is a direction for further experimental investigation.

Consistent with the analysis of macrophage and T lymphocyte abundance, mast cell abundance is also significantly higher in the intralobular stroma, compared to the more distant interlobular stroma (Fig. 6f - g). This is seen in both intact and neutered males. Similarly in the rat mammary gland mast cells tend to be located in the stroma surrounding the ducts (Ramirez et al., 2012). Mast cell number is also four times higher in the stroma adjacent to the mammary ducts, compared to more distant regions, in the female bovine mammary gland (Beaudry et al., 2016). This suggests that mammary mast cell localisation is similar between species and between males and females.

Conclusions

The ovine tissue analysed in this study was obtained from multiple sources from sheep with different genetic backgrounds and maintained with different husbandry practices. Additionally, tissue obtained from pubertal females was collected from sheep euthanised throughout the year and their stage of the oestrus cycle at the time of tissue collection is unknown. Together, this constitutes a heterogeneous sample population which introduces

bioRxiv preprint doi: https://doi.org/10.1101/2023.12.17.572059; this version posted December 17, 2023. The copyright holder for this preprint (which was not certified by peer review) is the author/funder, who has granted bioRxiv a license to display the preprint in perpetuity. It is made available under a CC-BY-NC-ND 4.0 International license.

388 considerable variability into the dataset. Arguably, this mirrors the heterogeneity in the
389 mammary microenvironment in the human population.

390

391 This study demonstrates the utility of the male ovine mammary gland as a tool to further our
392 understanding of postnatal male mammary biology. This vestigial glandular structure contains
393 a diverse set of immune cell types and exhibits distinct hormone receptor expression patterns,
394 features that in both cases are affected by neutered status. Interestingly, the immune
395 microenvironment of the male ovine gland appears to share features with that of the female
396 gland in sheep and other species. This observation, together with the well-documented histo-
397 anatomical similarities of the sheep mammary gland to the human breast (Hughes, 2021b;
398 Nagy et al., 2021; Rowson et al., 2012) indicate that the male sheep mammary gland may be
399 a useful adjunctive model of the male human breast. As mammary tumourigenesis is rare in
400 sheep (Hughes, 2021b; Newman et al., 2021), the male ovine gland does not offer a direct
401 model for male breast cancer, but it will facilitate furthering understanding of normal male
402 mammary biology to use in comparative studies. In addition, the relative resistance of the
403 sheep to development of mammary tumours may be a further fruitful avenue of future
404 comparative study (Hughes, 2023).

405

406 **Acknowledgements**

407 BPD is supported by an Anatomical Society PhD studentship awarded to KH. The authors
408 would like to thank Hugh Balmer, Yvonne Pratt, Andrea Starling and Emma Ward of the
409 Department of Veterinary Medicine, University of Cambridge, for their excellent technical
410 expertise in the preparation of tissue sections, and Mathew Rhodes, of the same department,
411 for technical assistance in the post mortem room. We acknowledge the Ethics and Welfare

bioRxiv preprint doi: https://doi.org/10.1101/2023.12.17.572059; this version posted December 17, 2023. The copyright holder for this preprint (which was not certified by peer review) is the author/funder, who has granted bioRxiv a license to display the preprint in perpetuity. It is made available under a CC-BY-NC-ND 4.0 International license.

412 Committee of the Department of Veterinary Medicine, University of Cambridge, for their
413 review of the study plan relating to the use of tissue from ovine post mortem examinations for
414 the study of mammary gland biology (references: CR223 and CR625). Parts of this data were
415 presented in oral abstract form at a the European Network for Breast Development and
416 Cancer online seminar series (presentation date 6 December 2022) and at the Anatomical
417 Society Summer Meeting 2023 in Bangor, Wales (25-27 July 2023; presentation date 25 July
418 2023).

419

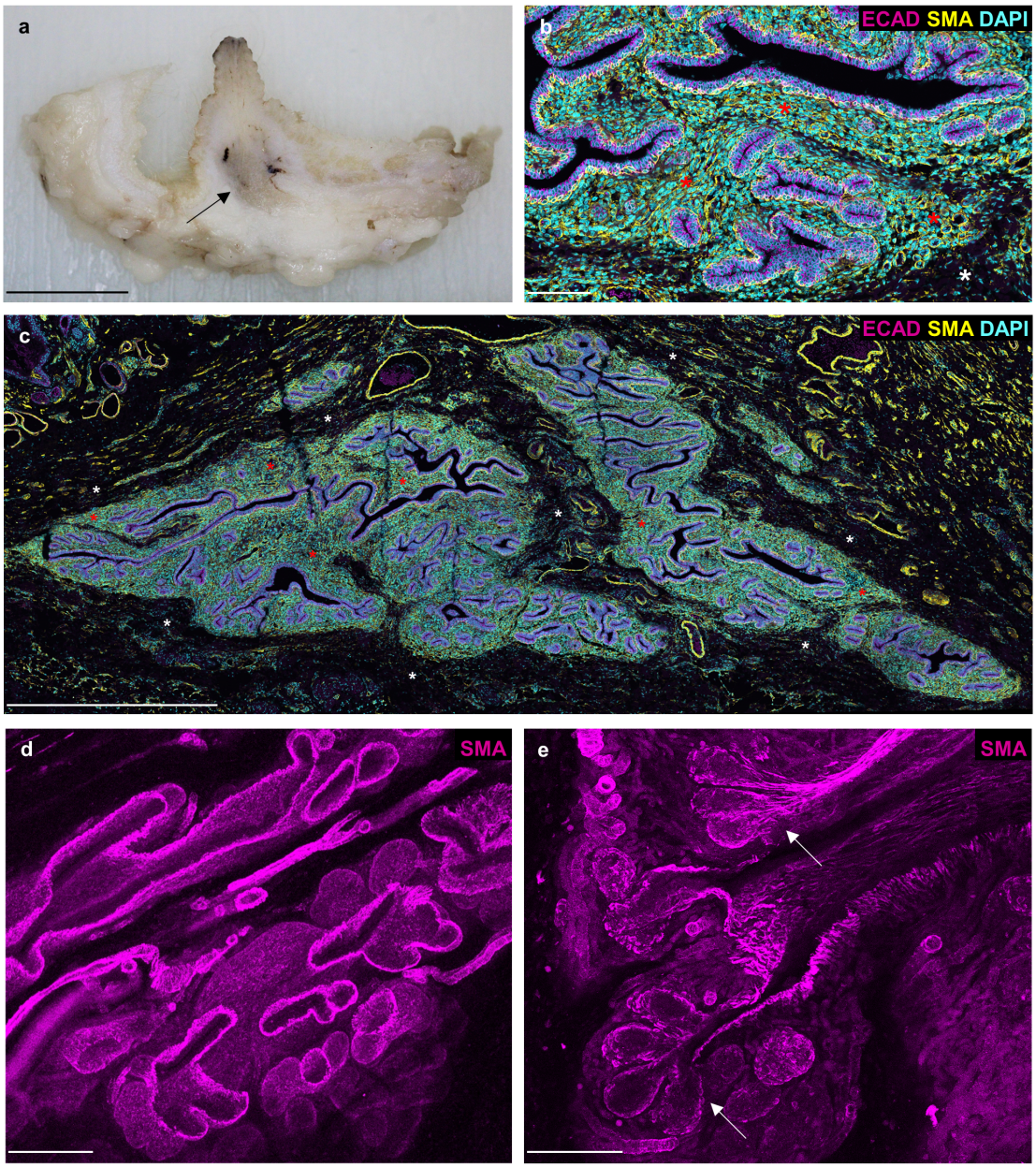
420 **Author contributions**

421 BPD and KH contributed to study concept and design. BPD, RCC, ALKC, KD, AFB, SJ, IM,
422 YN, BWS, KW, ALF, DAG and KH contributed to acquisition of data. BPD, CEB, JWW, and
423 KH contributed to data analysis and interpretation. BPD and KH drafted the manuscript. All
424 authors contributed to critical revision of the manuscript and approved the final version.

425

bioRxiv preprint doi: https://doi.org/10.1101/2023.12.17.572059; this version posted December 17, 2023. The copyright holder for this preprint (which was not certified by peer review) is the author/funder, who has granted bioRxiv a license to display the preprint in perpetuity. It is made available under a CC-BY-NC-ND 4.0 International license.

426 **Figures**



427

428 **Figure 1: Macro and histo-anatomy of the male ovine mammary gland.** (**a**) A sub-gross
429 image of fixed male ovine mammary tissue. Arrow indicates mammary gland. (**b**, **c**)
430 Immunofluorescence staining for luminal epithelial cells, using E-cadherin (magenta),
431 myoepithelial cells, using alpha-smooth muscle actin (yellow) and DNA, using DAPI (cyan).
432 Red asterisks indicate areas of intralobular mammary stroma. White asterisks indicate areas
433 of interlobular mammary stroma. (**d**, **e**) 3D maximum intensity projections of optically

bioRxiv preprint doi: https://doi.org/10.1101/2023.12.17.572059; this version posted December 17, 2023. The copyright holder for this preprint (which was not certified by peer review) is the author/funder, who has granted bioRxiv a license to display the preprint in perpetuity. It is made available under a CC-BY-NC-ND 4.0 International license.

434 cleared male ovine mammary tissue, using confocal microscopy. Immunofluorescence
435 staining for alpha-smooth muscle actin (magenta). Arrows indicate terminal duct lobular
436 units. Images are representative of 3 biological repeats Scale bar = 1 cm (**a**); 100 µm (**b**); 1
437 mm (**c**); 200 µm (**d**); 100 µm (**e**).

bioRxiv preprint doi: https://doi.org/10.1101/2023.12.17.572059; this version posted December 17, 2023. The copyright holder for this preprint (which was not certified by peer review) is the author/funder, who has granted bioRxiv a license to display the preprint in perpetuity. It is made available under a CC-BY-NC-ND 4.0 International license.

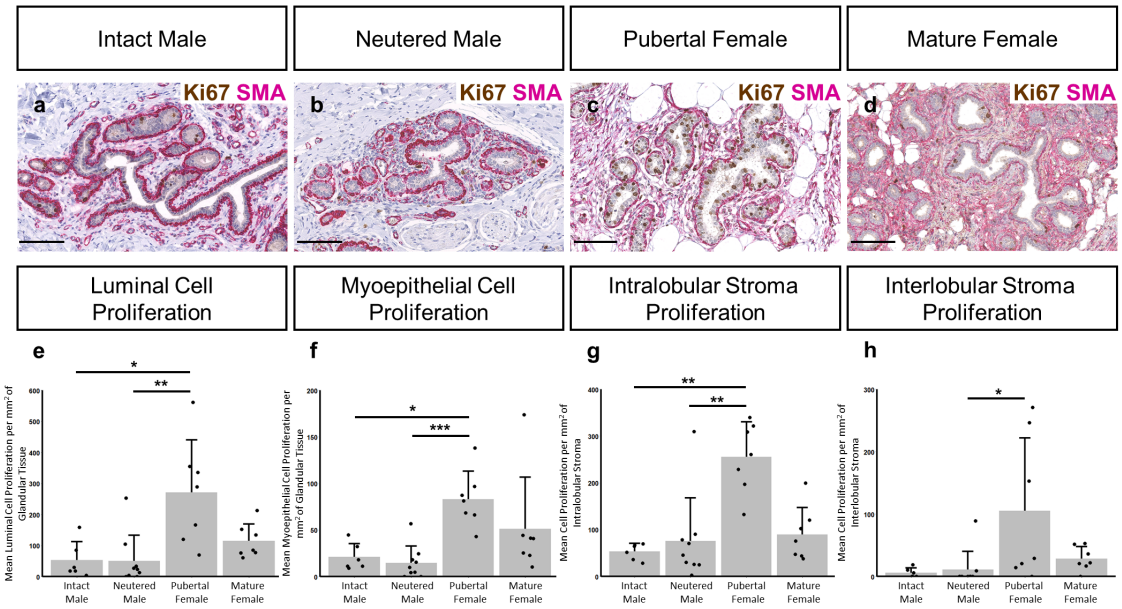


Figure 2: Proliferation dynamics within the intact male, neutered male, pubertal female and mature female mammary gland. (a-d) Dual immunohistochemical staining for Ki67 (brown) and alpha-SMA (magenta) in the mammary gland of intact males (**a**), neutered males (**b**), pubertal females (**c**) and mature females (**d**). (**e-h**) Bar graphs illustrating differences in mean luminal cell proliferation (**e**), myoepithelial cell proliferation (**f**), intralobular stroma proliferation (**g**) and interlobular stroma proliferation (**h**) per mm^2 of glandular tissue, intra- or interlobular mammary stroma + standard deviation ($*p< 0.05$, $**p< 0.01$, $***p< 0.001$, N= 6 for intact males, N =9 for neutered males, N= 7 for pubertal females, N = 7 for mature females, using Kruskal-Wallis test). Dots represent individual sheep. Images representative of 6 (**a**), 9 (**b**) and 7 (**c, d**) biological repeats. All IHC shown with a haematoxylin counterstain. Scale bar = 100 µm (**a-d**).

bioRxiv preprint doi: https://doi.org/10.1101/2023.12.17.572059; this version posted December 17, 2023. The copyright holder for this preprint (which was not certified by peer review) is the author/funder, who has granted bioRxiv a license to display the preprint in perpetuity. It is made available under a CC-BY-NC-ND 4.0 International license.

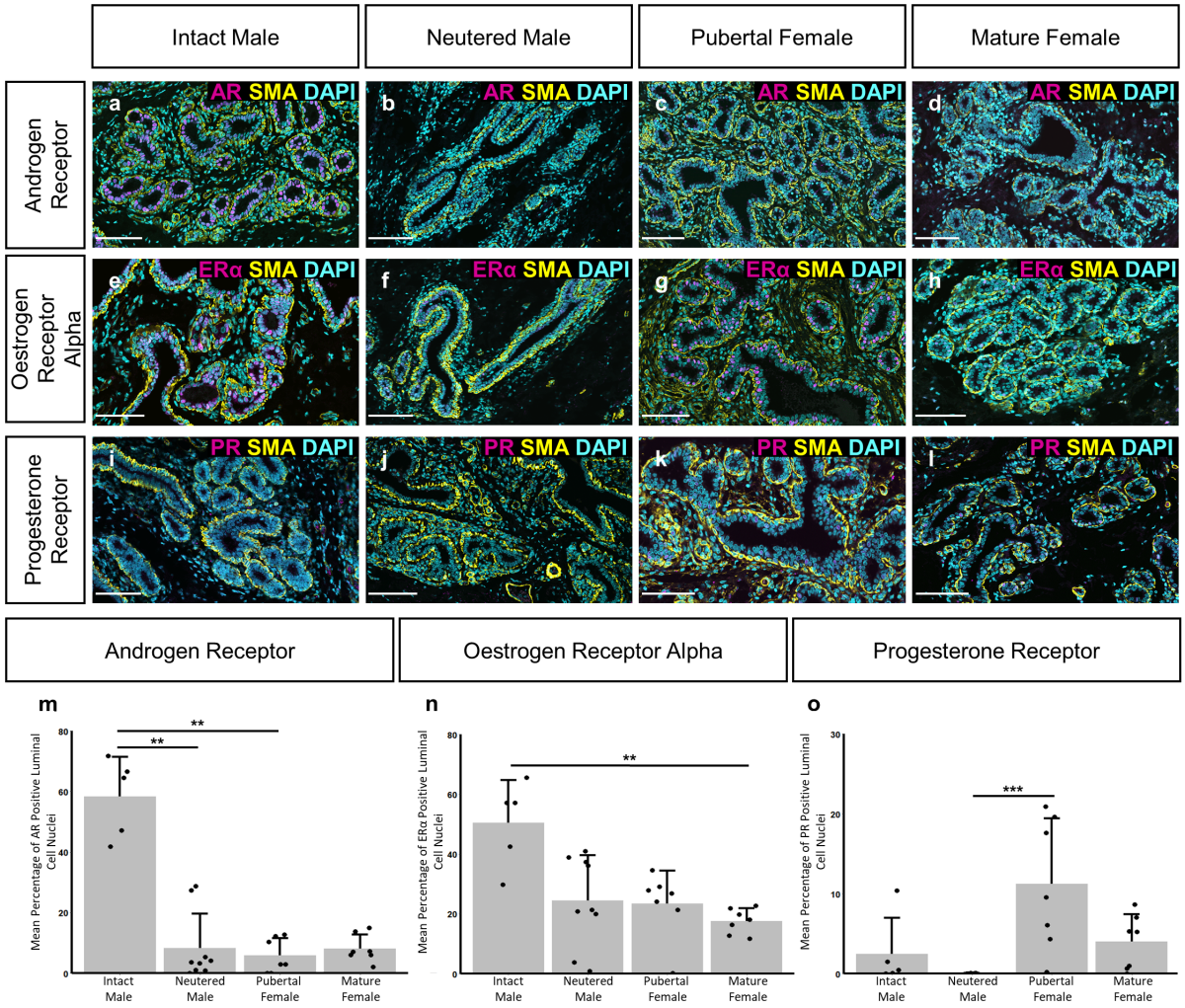


Figure 3: Differences in mammary epithelial hormone receptor expression between intact males, neutered males, pubertal females and mature females. (a-l) Immunofluorescence staining for androgen receptor (AR) **(a-d),** oestrogen receptor alpha (ERα) **(e-h)**, progesterone receptor A/B (PR) **(i-l)** (magenta), alpha-SMA (yellow) and DAPI (cyan) in the mammary gland of intact males (**a, e, i**), neutered males (**b, f, j**), pubertal females (**c, g, k**) and mature females (**d, h, l**). (**m-o**) Bar graphs illustrating differences in the mean percentage of AR (**m**), ERα (**n**) or PR (**o**) positive luminal cell nuclei + standard deviation (∗∗p< 0.01, ∗∗∗p< 0.001, N= 5 for intact males, N =9 for neutered males, N= 7 for pubertal females, N = 7 for mature females, using Kruskal-Wallis test). Dots represent

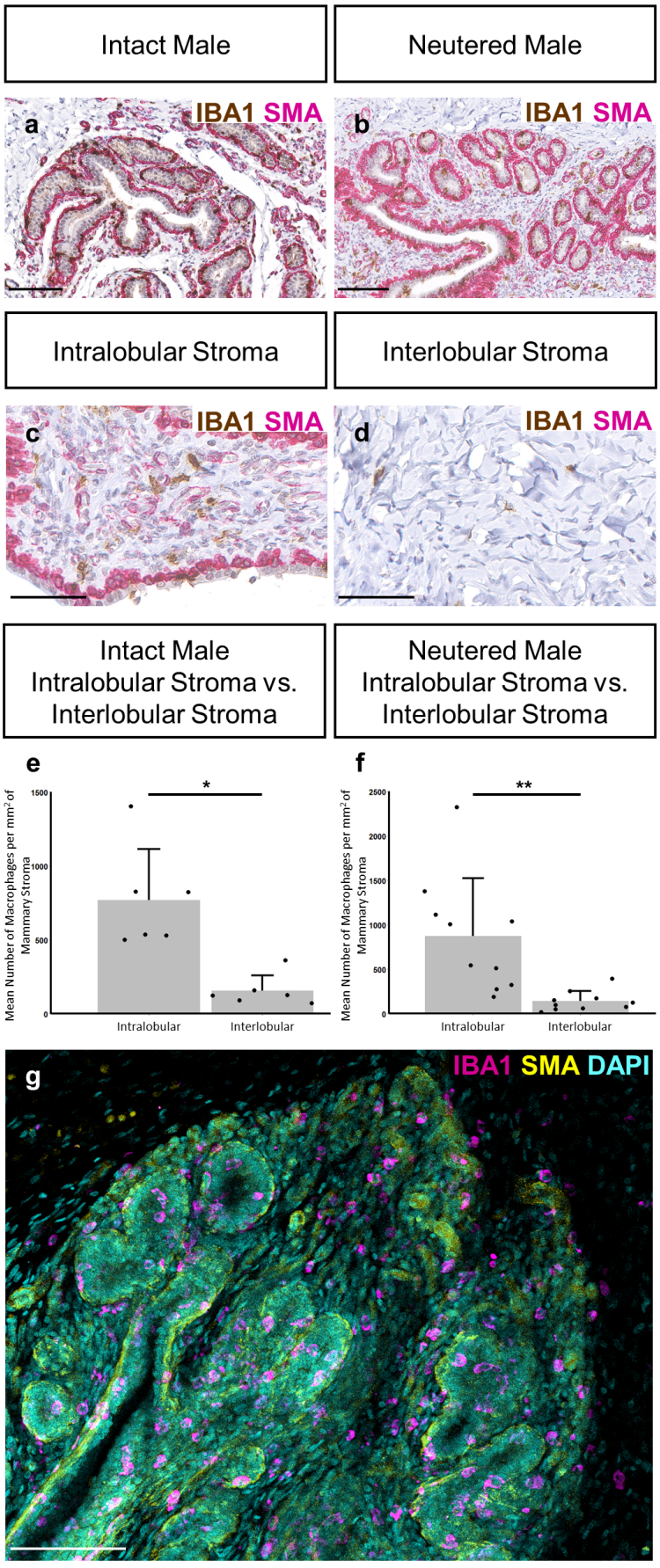
bioRxiv preprint doi: https://doi.org/10.1101/2023.12.17.572059; this version posted December 17, 2023. The copyright holder for this preprint (which was not certified by peer review) is the author/funder, who has granted bioRxiv a license to display the preprint in perpetuity. It is made available under a CC-BY-NC-ND 4.0 International license.

462 individual sheep. Images representative of 5 (**a, e, i**), 9 (**b, f, j**) and 7 (**c, d, g, h, k, l**)

463 biological repeats. Scale bar = 100 μm (**a-l**).

464

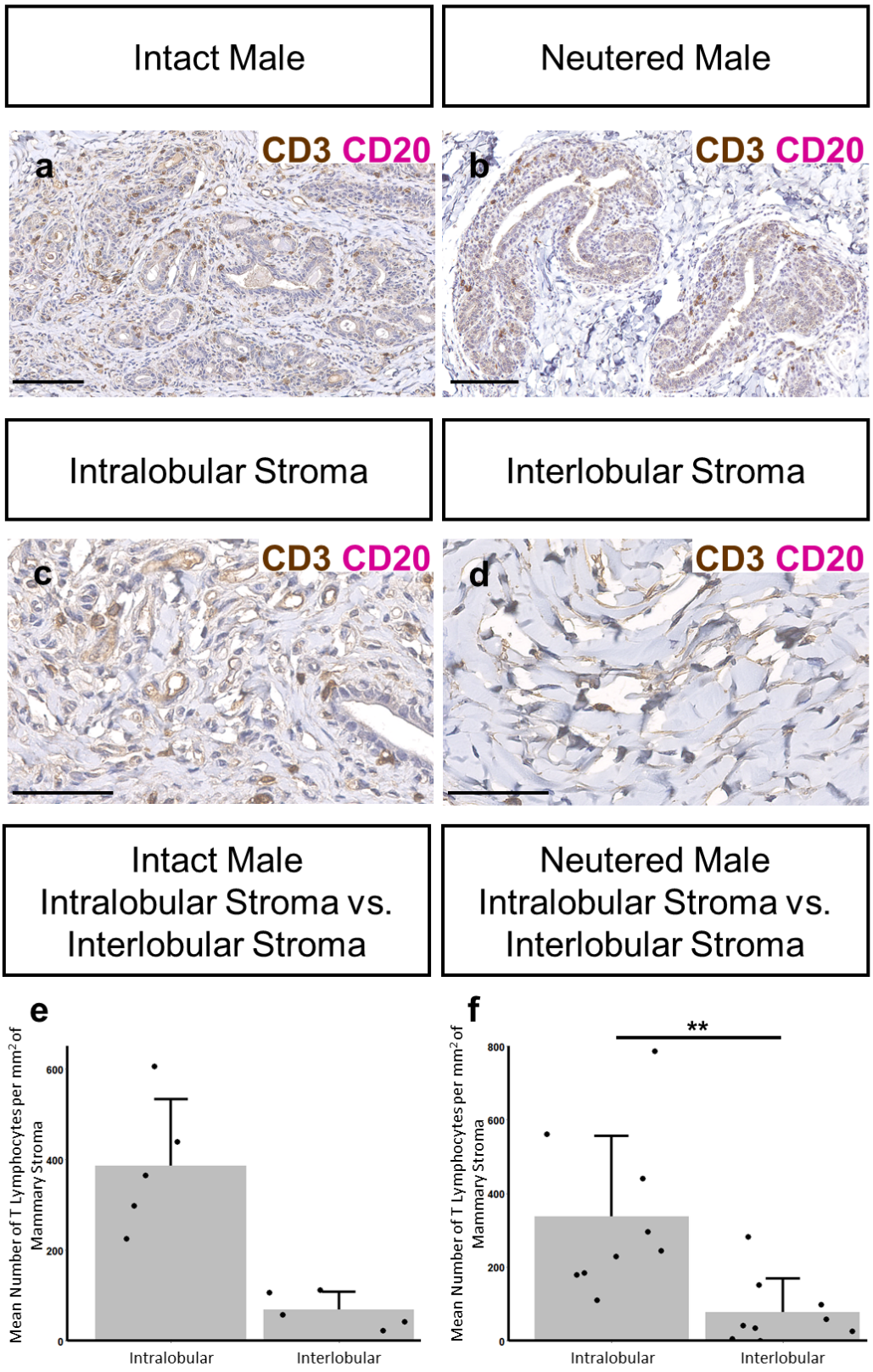
bioRxiv preprint doi: https://doi.org/10.1101/2023.12.17.572059; this version posted December 17, 2023. The copyright holder for this preprint (which was not certified by peer review) is the author/funder, who has granted bioRxiv a license to display the preprint in perpetuity. It is made available under a CC-BY-NC-ND 4.0 International license.



bioRxiv preprint doi: https://doi.org/10.1101/2023.12.17.572059; this version posted December 17, 2023. The copyright holder for this preprint (which was not certified by peer review) is the author/funder, who has granted bioRxiv a license to display the preprint in perpetuity. It is made available under a CC-BY-NC-ND 4.0 International license.

Figure 4: Macrophage abundance and localisation within the intact and neutered male ovine mammary gland. (a-d) Dual immunohistochemical staining for IBA1 (brown) and alpha-SMA (magenta) in the mammary gland of intact males (**a**) and neutered males (**b**). (**c-d**) The abundance of macrophages in the intralobular (**c**) and interlobular mammary stroma (**d**). (**e, f**) Bar graphs illustrating differences in the mean number of macrophages per mm^2 of mammary stroma in the intralobular and interlobular stroma of intact (**e**) and neutered males (**f**) + standard deviation ($*p< 0.05$, $**p< 0.01$, N= 6 for intact males, N =10 for neutered males, using Wilcoxon signed-rank test). Dots represent individual sheep. (**g**) A 3D maximum intensity projection of optically cleared male ovine mammary tissue, using confocal microscopy. Immunofluorescence staining for IBA1 (magenta), alpha-SMA (yellow) and DAPI (cyan). Images representative of 6 (**a**), 10 (**b, c, d**) and 3 (**g**) biological repeats. Scale bar = 100 µm (**a, b, g**); 50 µm (**c, d**).

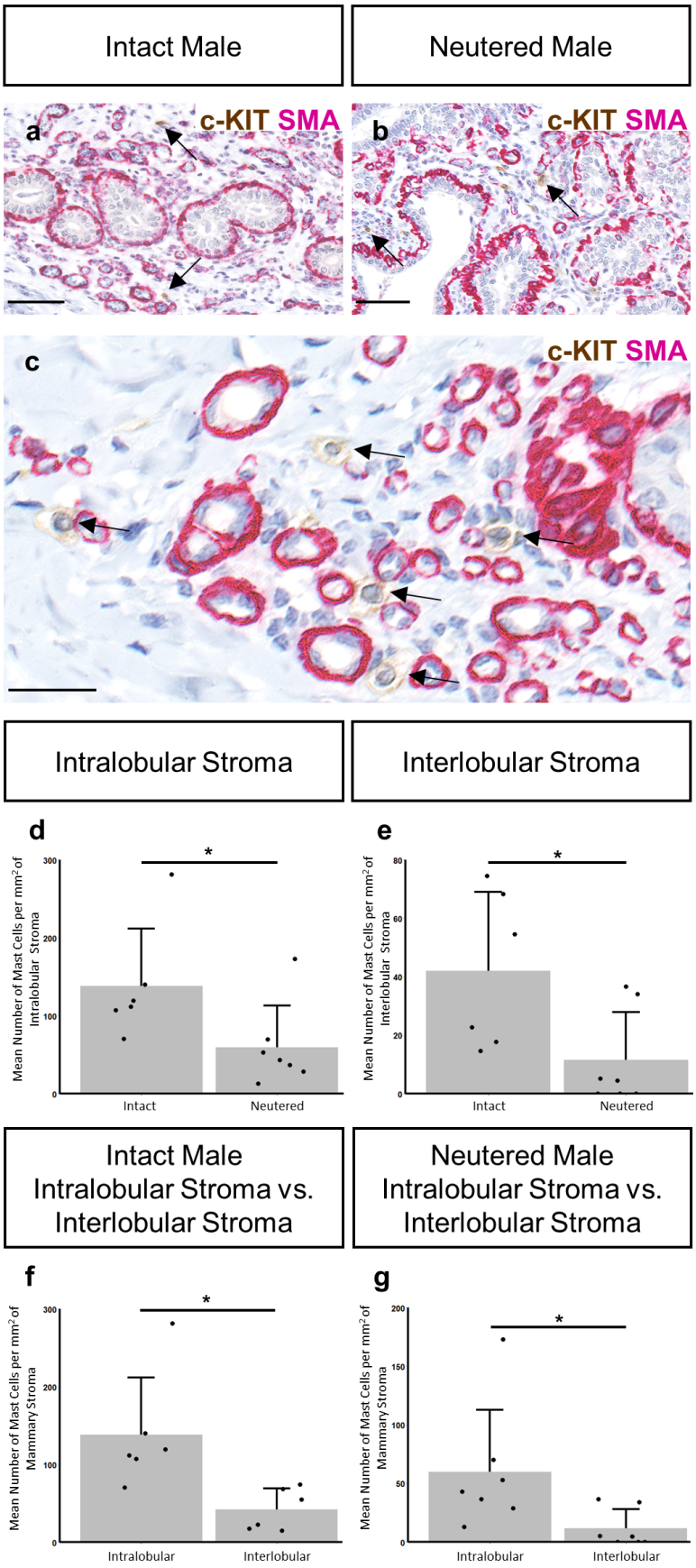
bioRxiv preprint doi: https://doi.org/10.1101/2023.12.17.572059; this version posted December 17, 2023. The copyright holder for this preprint (which was not certified by peer review) is the author/funder, who has granted bioRxiv a license to display the preprint in perpetuity. It is made available under a CC-BY-NC-ND 4.0 International license.



bioRxiv preprint doi: https://doi.org/10.1101/2023.12.17.572059; this version posted December 17, 2023. The copyright holder for this preprint (which was not certified by peer review) is the author/funder, who has granted bioRxiv a license to display the preprint in perpetuity. It is made available under a CC-BY-NC-ND 4.0 International license.

Figure 5: T- lymphocyte abundance within the intact and neutered male ovine mammary gland. (a-d) Dual immunohistochemical staining for CD3 (brown) and CD20 (magenta) in the mammary gland of intact males (**a**) and neutered males (**b**) and within the intralobular (**c**) and interlobular mammary stroma (**d**). (**e, f**) Bar graphs illustrating differences in the mean number of T- lymphocytes per mm^2 of mammary stroma in the intralobular and interlobular stroma of intact (**e**) and neutered males (**f**) + standard deviation (∗∗$p < 0.01$, N= 5 for intact males, N =9 for neutered males, using Wilcoxon signed-rank test). Dots represent individual sheep. Images representative of 5 (**a, c, d**) and 9 (**b**) biological repeats. All IHC shown with a haematoxylin counterstain. Scale bar = 100 µm (**a, b**); 50 µm (**c, d**).

bioRxiv preprint doi: https://doi.org/10.1101/2023.12.17.572059; this version posted December 17, 2023. The copyright holder for this preprint (which was not certified by peer review) is the author/funder, who has granted bioRxiv a license to display the preprint in perpetuity. It is made available under a CC-BY-NC-ND 4.0 International license.



bioRxiv preprint doi: https://doi.org/10.1101/2023.12.17.572059; this version posted December 17, 2023. The copyright holder for this preprint (which was not certified by peer review) is the author/funder, who has granted bioRxiv a license to display the preprint in perpetuity. It is made available under a CC-BY-NC-ND 4.0 International license.

Figure 6: Mast cells abundance is significantly higher in intact males. (a-c) Dual immunohistochemical staining for c-Kit (brown) and alpha-SMA (magenta) in the mammary gland of intact males (**a**) and neutered males (**b**). Arrows indicate positive staining for mast cells. (**c**) Mast cells are located in close proximity to blood vessels in the male ovine mammary gland. Arrows indicate positive mast cell staining. (**d, e**) Bar graphs illustrating differences in the mean number of mast cells per mm^2 of intralobular (**d**) and interlobular (**e**) stroma in intact and neutered males + standard deviation ($*p< 0.05$, N= 6 for intact males, N =7 for neutered males, using Mann-Whitney U test). (**f, g**) Bar graphs illustrating differences in the mean number of mast cells per mm^2 of mammary stroma in the intralobular and interlobular stroma of intact (**f**) and neutered males (**g**) + standard deviation ($*p< 0.05$, N= 6 for intact males, N =7 for neutered males, using Wilcoxon signed-rank test). Dots represent individual sheep. Images representative of 6 (**a, c**) and 7 (**b**) biological repeats. All IHC shown with a haematoxylin counterstain. Scale bar = 50 µm (**a, b**); 25 µm (**c**).

bioRxiv preprint doi: https://doi.org/10.1101/2023.12.17.572059; this version posted December 17, 2023. The copyright holder for this preprint (which was not certified by peer review) is the author/funder, who has granted bioRxiv a license to display the preprint in perpetuity. It is made available under a CC-BY-NC-ND 4.0 International license.

514 **References**

515 Atwood, C.S., Hovey, R.C., Glover, J.P., Chepko, G., Ginsburg, E., Robison, W.G.,
516 Vonderhaar, B.K., 2000. Progesterone induces side-branching of the ductal epithelium in the
517 mammary glands of peripubertal mice. Journal of Endocrinology 167, 39–52.
518 https://doi.org/10.1677/joe.0.1670039

519 Beaudry, K.L., Parsons, C.L.M., Ellis, S.E., Akers, R.M., 2016. Localization and quantitation
520 of macrophages, mast cells, and eosinophils in the developing bovine mammary gland1.
521 Journal of Dairy Science 99, 796–804. https://doi.org/10.3168/jds.2015-9972

522 Brisken, C., Park, S., Vass, T., Lydon, J.P., O'Malley, B.W., Weinberg, R.A., 1998. A
523 paracrine role for the epithelial progesterone receptor in mammary gland development. Proc
524 Natl Acad Sci U S A 95, 5076–5081.

525 Cardiff, R.D., Jindal, S., Treuting, P.M., Going, J.J., Gusterson, B., Thompson, H.J., 2018. 23
526 - Mammary Gland, in: Treuting, P.M., Dintzis, S.M., Montine, K.S. (Eds.), Comparative
527 Anatomy and Histology (Second Edition). Academic Press, San Diego, pp. 487–509.
528 https://doi.org/10.1016/B978-0-12-802900-8.00023-3

529 Cardoso, F., Bartlett, J.M.S., Slaets, L., van Deurzen, C.H.M., van Leeuwen-Stok, E., Porter,
530 P., Linderholm, B., Hedenfalk, I., Schröder, C., Martens, J., Bayani, J., van Asperen, C.,
531 Murray, M., Hudis, C., Middleton, L., Vermeij, J., Punie, K., Fraser, J., Nowaczyk, M.,
532 Rubio, I.T., Aebi, S., Kelly, C., Ruddy, K.J., Winer, E., Nilsson, C., Lago, L.D., Korde, L.,
533 Benstead, K., Bogler, O., Goulioti, T., Peric, A., Litière, S., Aalders, K.C., Poncet, C.,
534 Tryfonidis, K., Giordano, S.H., 2018. Characterization of male breast cancer: results of the
535 EORTC 10085/TBCRC/BIG/NABCG International Male Breast Cancer Program. Annals of
536 Oncology, Incorporating blood-based liquid biopsy information into cancer staging 29, 405–
537 417. https://doi.org/10.1093/annonc/mdx651

bioRxiv preprint doi: https://doi.org/10.1101/2023.12.17.572059; this version posted December 17, 2023. The copyright holder for this preprint (which was not certified by peer review) is the author/funder, who has granted bioRxiv a license to display the preprint in perpetuity. It is made available under a CC-BY-NC-ND 4.0 International license.

538 Chatterji, S., Krzoska, E., Thoroughgood, C.W., Saganty, J., Liu, P., Elsberger, B., Abu-Eid,
539 R., Speirs, V., 2023. Defining genomic, transcriptomic, proteomic, epigenetic, and phenotypic
540 biomarkers with prognostic capability in male breast cancer: a systematic review. The Lancet
541 Oncology 24, e74–e85. https://doi.org/10.1016/S1470-2045(22)00633-7

542 Chen, W., Beck, I., Schober, W., Brockow, K., Effner, R., Buters, J.T.M., Behrendt, H., Ring,
543 J., 2010. Human mast cells express androgen receptors but treatment with testosterone exerts
544 no influence on IgE-independent mast cell degranulation elicited by neuromuscular blocking
545 agents. Experimental Dermatology 19, 302–304. https://doi.org/10.1111/j.1600-
546 0625.2009.00969.x

547 Chua, A.C.L., Hodson, L.J., Moldenhauer, L.M., Robertson, S.A., Ingman, W.V., 2010. Dual
548 roles for macrophages in ovarian cycle-associated development and remodelling of the
549 mammary gland epithelium. Development 137, 4229–4238.
550 https://doi.org/10.1242/dev.059261

551 Colitti, M., Parillo, F., 2013. Immunolocalization of estrogen and progesterone receptors in
552 ewe mammary glands. Microscopy Research and Technique 76, 955–962.
553 https://doi.org/10.1002/jemt.22254

554 Dawson, C.A., Pal, B., Vaillant, F., Gandolfo, L.C., Liu, Z., Bleriot, C., Ginhoux, F., Smyth,
555 G.K., Lindeman, G.J., Mueller, S.N., Rios, A.C., Visvader, J.E., 2020. Tissue-resident ductal
556 macrophages survey the mammary epithelium and facilitate tissue remodelling. Nat Cell Biol
557 22, 546–558. https://doi.org/10.1038/s41556-020-0505-0

558 Dimitrakakis, C., Bondy, C., 2009. Androgens and the breast. Breast Cancer Research 11,
559 212. https://doi.org/10.1186/bcr2413

bioRxiv preprint doi: https://doi.org/10.1101/2023.12.17.572059; this version posted December 17, 2023. The copyright holder for this preprint (which was not certified by peer review) is the author/funder, who has granted bioRxiv a license to display the preprint in perpetuity. It is made available under a CC-BY-NC-ND 4.0 International license.

560 Drews, Ulrich, Drews, Ute, 1977. Regression of mouse mammary gland anlagen in
561 recombinants of Tfm and wild-type tissues: testosterone acts via the mesenchyme. Cell 10,
562 401–404. https://doi.org/10.1016/0092-8674(77)90027-7

563 Dürnberger, H., Kratochwil, K., 1980. Specificity of tissue interaction and origin of
564 mesenchymal cells in the androgen response of the embryonic mammary gland. Cell 19, 465–
565 471. https://doi.org/10.1016/0092-8674(80)90521-8

566 Fox, S., Speirs, V., Shaaban, A.M., 2022. Male breast cancer: an update. Virchows Arch 480,
567 85–93. https://doi.org/10.1007/s00428-021-03190-7

568 Gao, Y.R. (Ellen), Walters, K.A., Desai, R., Zhou, H., Handelsman, D.J., Simanainen, U.,
569 2014. Androgen Receptor Inactivation Resulted in Acceleration in Pubertal Mammary Gland
570 Growth, Upregulation of ERα Expression, and Wnt/β-Catenin Signaling in Female Mice.
571 Endocrinology 155, 4951–4963. https://doi.org/10.1210/en.2014-1226

572 Hassiotou, F., Geddes, D., 2013. Anatomy of the human mammary gland: Current status of
573 knowledge. Clin. Anat. 26, 29–48. https://doi.org/10.1002/ca.22165

574 Hilton, H.N., Graham, J.D., Clarke, C.L., 2015. Minireview: Progesterone Regulation of
575 Proliferation in the Normal Human Breast and in Breast Cancer: A Tale of Two Scenarios?
576 Molecular Endocrinology 29, 1230–1242. https://doi.org/10.1210/me.2015-1152

577 Hodson, L.J., Chua, A.C.L., Evdokiou, A., Robertson, S.A., Ingman, W.V., 2013. Macrophage
578 Phenotype in the Mammary Gland Fluctuates over the Course of the Estrous Cycle and Is
579 Regulated by Ovarian Steroid Hormones1. Biology of Reproduction 89, 65, 1–8.
580 https://doi.org/10.1095/biolreprod.113.109561

bioRxiv preprint doi: https://doi.org/10.1101/2023.12.17.572059; this version posted December 17, 2023. The copyright holder for this preprint (which was not certified by peer review) is the author/funder, who has granted bioRxiv a license to display the preprint in perpetuity. It is made available under a CC-BY-NC-ND 4.0 International license.

581 Hovey, R.C., Mcfadden, T.B., Akers, R.M., 1999. Regulation of Mammary Gland Growth
582 and Morphogenesis by the Mammary Fat Pad: A Species Comparison. J Mammary Gland
583 Biol Neoplasia 4, 53–68. https://doi.org/10.1023/A:1018704603426

584 Hughes, K., 2023. Studying Mammary Physiology and Pathology in Domestic Species
585 Benefits Both Humans and Animals. J Mammary Gland Biol Neoplasia 28, 18.
586 https://doi.org/10.1007/s10911-023-09547-9

587 Hughes, K., 2021a. Development and Pathology of the Equine Mammary Gland. J Mammary
588 Gland Biol Neoplasia 26, 121–134. https://doi.org/10.1007/s10911-020-09471-2

589 Hughes, K., 2021b. Comparative mammary gland postnatal development and tumourigenesis
590 in the sheep, cow, cat and rabbit: Exploring the menagerie. Semin Cell Dev Biol 114, 186–
591 195. https://doi.org/10.1016/j.semcdb.2020.09.010

592 Hughes, K., Watson, C.J., 2018. The Mammary Microenvironment in Mastitis in Humans,
593 Dairy Ruminants, Rabbits and Rodents: A One Health Focus. J Mammary Gland Biol
594 Neoplasia 23, 27–41. https://doi.org/10.1007/s10911-018-9395-1

595 Hughes, K., Wickenden, J.A., Allen, J.E., Watson, C.J., 2012. Conditional deletion of Stat3 in
596 mammary epithelium impairs the acute phase response and modulates immune cell numbers
597 during post-lactational regression. The Journal of Pathology 227, 106–117.
598 https://doi.org/10.1002/path.3961

599 Inman, J.L., Robertson, C., Mott, J.D., Bissell, M.J., 2015. Mammary gland development:
600 cell fate specification, stem cells and the microenvironment. Development 142, 1028–1042.
601 https://doi.org/10.1242/dev.087643

602 Iuanow, E., Kettler, M., Slanetz, P.J., 2011. Spectrum of Disease in the Male Breast.
603 American Journal of Roentgenology 196, W247–W259. https://doi.org/10.2214/AJR.09.3994

bioRxiv preprint doi: https://doi.org/10.1101/2023.12.17.572059; this version posted December 17, 2023. The copyright holder for this preprint (which was not certified by peer review) is the author/funder, who has granted bioRxiv a license to display the preprint in perpetuity. It is made available under a CC-BY-NC-ND 4.0 International license.

604 Jenkinson, C.M.C., 2003. The pattern and regulation of mammary gland development during
605 fetal life in sheep : a thesis presented in partial fulfilment of the requirements for the degree
606 of Doctor of Philosophy in Animal Science at Massey University, Palmerston North, New
607 Zealand. Massey University.

608 Jesinger, R.A., 2014. Breast Anatomy for the Interventionalist. Techniques in Vascular and
609 Interventional Radiology, Breast Interventions 17, 3–9.
610 https://doi.org/10.1053/j.tvir.2013.12.002

611 Kolla, S., Pokharel, A., Vandenberg, L.N., 2017. The mouse mammary gland as a sentinel
612 organ: distinguishing 'control' populations with diverse environmental histories. Environ
613 Health 16, 25. https://doi.org/10.1186/s12940-017-0229-1

614 Lammie, A., Drobnjak, M., Gerald, W., Saad, A., Cote, R., Cordon-Cardo, C., 1994.
615 Expression of c-kit and kit ligand proteins in normal human tissues. Journal of
616 Histochemistry & Cytochemistry 42, 1417–1425. https://doi.org/10.1177/42.11.7523489

617 Lilla, J.N., Werb, Z., 2010. Mast cells contribute to the stromal microenvironment in
618 mammary gland branching morphogenesis. Developmental Biology 337, 124–133.
619 https://doi.org/10.1016/j.ydbio.2009.10.021

620 Liu, N., Johnson, K.J., Ma, C.X., 2018. Male Breast Cancer: An Updated Surveillance,
621 Epidemiology, and End Results Data Analysis. Clinical Breast Cancer 18, e997–e1002.
622 https://doi.org/10.1016/j.clbc.2018.06.013

623 Liva, S.M., Voskuhl, R.R., 2001. Testosterone Acts Directly on CD4+ T Lymphocytes to
624 Increase IL-10 Production1. The Journal of Immunology 167, 2060–2067.
625 https://doi.org/10.4049/jimmunol.167.4.2060

bioRxiv preprint doi: https://doi.org/10.1101/2023.12.17.572059; this version posted December 17, 2023. The copyright holder for this preprint (which was not certified by peer review) is the author/funder, who has granted bioRxiv a license to display the preprint in perpetuity. It is made available under a CC-BY-NC-ND 4.0 International license.

626 Lloyd-Lewis, B., Davis, F.M., Harris, O.B., Hitchcock, J.R., Lourenco, F.C., Pasche, M.,
627 Watson, C.J., 2016. Imaging the mammary gland and mammary tumours in 3D: optical tissue
628 clearing and immunofluorescence methods. Breast Cancer Research 18, 127.
629 https://doi.org/10.1186/s13058-016-0754-9

630 Macias, H., Hinck, L., 2012. Mammary gland development. WIREs Developmental Biology
631 1, 533–557. https://doi.org/10.1002/wdev.35

632 Morrison, J., Berry, M., Botting, K., Darby, J., Frasch, M., Gatford, K., Giussani, D., Gray,
633 C., Harding, R., Herrera, E., Kemp, M., Lock, M., Mcmillen, I., Moss, T., Musk, G., Oliver,
634 M., Regnault, T., Roberts, C., Soo, J., Tellam, R., 2018. Improving pregnancy outcomes in
635 humans through studies in sheep. American Journal of Physiology-Regulatory, Integrative
636 and Comparative Physiology 315. https://doi.org/10.1152/ajpregu.00391.2017

637 Nagy, D., Gillis, C.M.C., Davies, K., Fowden, A.L., Rees, P., Wills, J.W., Hughes, K., 2021.
638 Developing ovine mammary terminal duct lobular units have a dynamic mucosal and stromal
639 immune microenvironment. Commun Biol 4, 993. https://doi.org/10.1038/s42003-021-
640 02502-6

641 Newman, S.J., Smith, S.A., Zimmerman, K., 2021. Mammary carcinoma arising in an
642 adenoma in a ewe. J Vet Diagn Invest 33, 566–571.
643 https://doi.org/10.1177/1040638721993061

644 Paine, I.S., Lewis, M.T., 2017. The Terminal End Bud: the Little Engine that Could. J
645 Mammary Gland Biol Neoplasia 22, 93–108. https://doi.org/10.1007/s10911-017-9372-0

646 Pokharel, A., Kolla, S., Matouskova, K., Vandenberg, L.N., 2018. Asymmetric development
647 of the male mouse mammary gland and its response to a prenatal or postnatal estrogen
648 challenge. Reprod Toxicol 82, 63–71. https://doi.org/10.1016/j.reprotox.2018.10.003

bioRxiv preprint doi: https://doi.org/10.1101/2023.12.17.572059; this version posted December 17, 2023. The copyright holder for this preprint (which was not certified by peer review) is the author/funder, who has granted bioRxiv a license to display the preprint in perpetuity. It is made available under a CC-BY-NC-ND 4.0 International license.

649 Ramirez, R.A., Lee, A., Schedin, P., Russell, J.S., Masso-Welch, P.A., 2012. Alterations in
650 mast cell frequency and relationship to angiogenesis in the rat mammary gland during
651 windows of physiologic tissue remodeling. Developmental Dynamics 241, 890–900.
652 https://doi.org/10.1002/dvdy.23778

653 Renfree, M.B., Robinson, E.S., Short, R.V., Vandeberg, J.L., 1990. Mammary glands in male
654 marsupials: I. Primordia in neonatal opossums Didelphis virginiana and Monodelphis
655 domestica. Development 110, 385–390. https://doi.org/10.1242/dev.110.2.385

656 Ribatti, D., 2018. The Staining of Mast Cells: A Historical Overview. International Archives
657 of Allergy and Immunology 176, 55–60. https://doi.org/10.1159/000487538

658 Richert, M.M., Schwertfeger, K.L., Ryder, J.W., Anderson, S.M., 2000. An Atlas of Mouse
659 Mammary Gland Development. J Mammary Gland Biol Neoplasia 5, 227–241.
660 https://doi.org/10.1023/A:1026499523505

661 Rowson, A.R., Daniels, K.M., Ellis, S.E., Hovey, R.C., 2012. Growth and development of the
662 mammary glands of livestock: A veritable barnyard of opportunities. Seminars in Cell &
663 Developmental Biology, Cell Regulation by Selective Protein Degradation & Biology of
664 Mammary Gland Development 23, 557–566. https://doi.org/10.1016/j.semcdb.2012.03.018

665 Safayi, S., Korn, N., Bertram, A., Akers, R.M., Capuco, A.V., Pratt, S.L., Ellis, S., 2012.
666 Myoepithelial cell differentiation markers in prepubertal bovine mammary gland: Effect of
667 ovariectomy. Journal of Dairy Science 95, 2965–2976. https://doi.org/10.3168/jds.2011-4690

668 Schindelin, J., Arganda-Carreras, I., Frise, E., Kaynig, V., Longair, M., Pietzsch, T., Preibisch,
669 S., Rueden, C., Saalfeld, S., Schmid, B., Tinevez, J.-Y., White, D.J., Hartenstein, V., Eliceiri,
670 K., Tomancak, P., Cardona, A., 2012. Fiji: an open-source platform for biological-image
671 analysis. Nature Methods 9, 676–682. https://doi.org/10.1038/nmeth.2019

bioRxiv preprint doi: https://doi.org/10.1101/2023.12.17.572059; this version posted December 17, 2023. The copyright holder for this preprint (which was not certified by peer review) is the author/funder, who has granted bioRxiv a license to display the preprint in perpetuity. It is made available under a CC-BY-NC-ND 4.0 International license.

672 Simanainen, U., Gao, Y.R., Walters, K.A., Watson, G., Desai, R., Jimenez, M., Handelsman,
673 D.J., 2012. Androgen Resistance in Female Mice Increases Susceptibility to DMBA-Induced
674 Mammary Tumors. Hormones and Cancer 3, 113–124. https://doi.org/10.1007/s12672-012-
675 0107-9

676 Stewart, T.A., Hughes, K., Hume, D.A., Davis, F.M., 2019. Developmental Stage-Specific
677 Distribution of Macrophages in Mouse Mammary Gland. Frontiers in Cell and
678 Developmental Biology 7, 250. https://doi.org/10.3389/fcell.2019.00250

679 Susaki, E.A., Tainaka, K., Perrin, D., Kishino, F., Tawara, T., Watanabe, T.M., Yokoyama, C.,
680 Onoe, H., Eguchi, M., Yamaguchi, S., Abe, T., Kiyonari, H., Shimizu, Y., Miyawaki, A.,
681 Yokota, H., Ueda, H.R., 2014. Whole-Brain Imaging with Single-Cell Resolution Using
682 Chemical Cocktails and Computational Analysis. Cell 157, 726–739.
683 https://doi.org/10.1016/j.cell.2014.03.042

684 Szabo, G.K., Vandenberg, L.N., 2021. REPRODUCTIVE TOXICOLOGY: The male
685 mammary gland: a novel target of endocrine-disrupting chemicals. Reproduction 162, F79–
686 F89. https://doi.org/10.1530/REP-20-0615

687 Tower, H., Dall, G., Davey, A., Stewart, M., Lanteri, P., Ruppert, M., Lambouras, M., Nasir,
688 I., Yeow, S., Darcy, P.K., Ingman, W.V., Parker, B., Haynes, N.M., Britt, K.L., 2022.
689 Estrogen-induced immune changes within the normal mammary gland. Scientific Reports 12,
690 18986. https://doi.org/10.1038/s41598-022-21871-4

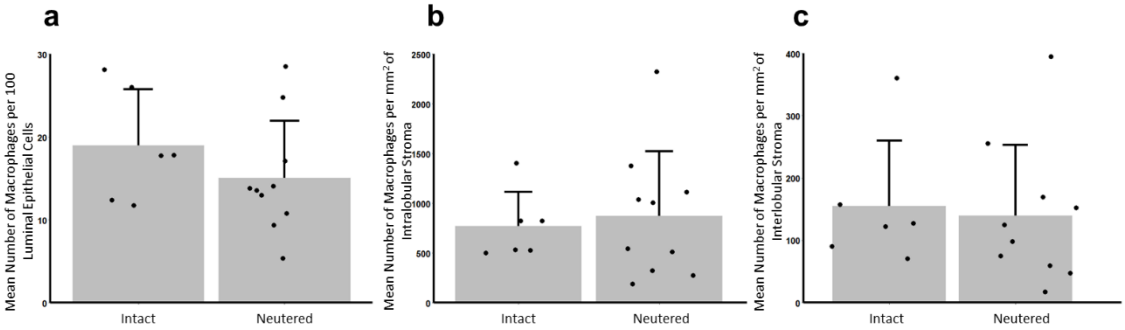
691 Vandenberg, L.N., Schaeberle, C.M., Rubin, B.S., Sonnenschein, C., Soto, A.M., 2013. The
692 male mammary gland: A target for the xenoestrogen bisphenol A. Reproductive Toxicology
693 37, 15–23. https://doi.org/10.1016/j.reprotox.2013.01.002

694

695

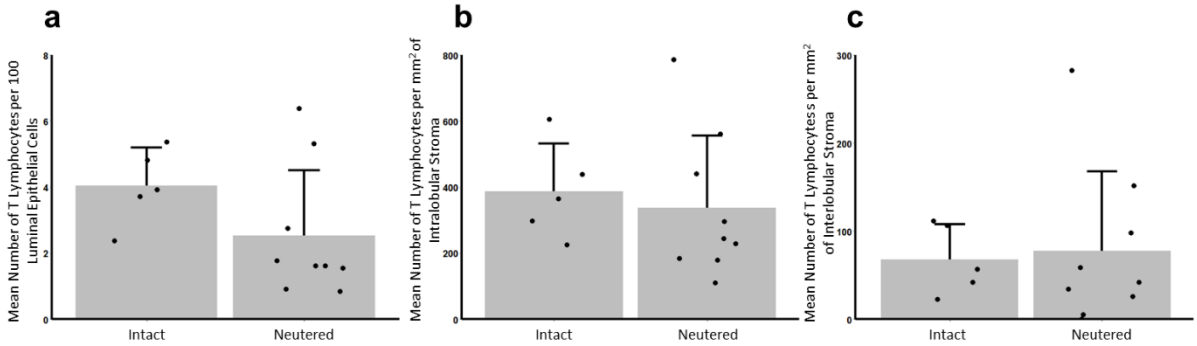
bioRxiv preprint doi: https://doi.org/10.1101/2023.12.17.572059; this version posted December 17, 2023. The copyright holder for this preprint (which was not certified by peer review) is the author/funder, who has granted bioRxiv a license to display the preprint in perpetuity. It is made available under a CC-BY-NC-ND 4.0 International license.

Supplementary Material



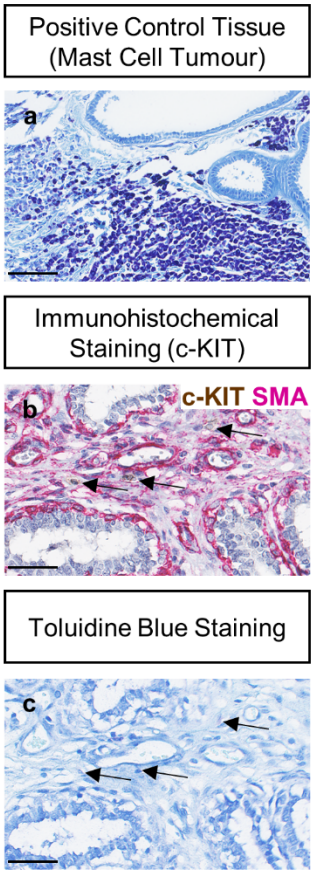
Supplementary Figure 1: There is no significant difference in macrophage abundance in the mammary glands of intact and neutered males. (a- c) Bar graphs illustrating differences, between intact and neutered males, in the mean number of macrophages per 100 luminal epithelial cells (a) and the mean number of macrophages per mm^2 of intralobular (b) or interlobular (c) + standard deviation (N= 6 for intact males, N =10 for neutered males, using Mann-Whitney U test). Dots represent individual sheep.

bioRxiv preprint doi: https://doi.org/10.1101/2023.12.17.572059; this version posted December 17, 2023. The copyright holder for this preprint (which was not certified by peer review) is the author/funder, who has granted bioRxiv a license to display the preprint in perpetuity. It is made available under a CC-BY-NC-ND 4.0 International license.



Supplementary Figure 2: There is no significant difference in T-lymphocyte abundance in the mammary glands of intact and neutered males. (a- c) Bar graphs illustrating differences, between intact and neutered males, in the mean number of T-lymphocytes per 100 luminal epithelial cells (a) and the mean number of T-lymphocytes per mm^2 of intralobular (b) or interlobular (c) + standard deviation (N= 5 for intact males, N =9 for neutered males, using Mann-Whitney U test). Dots represent individual sheep.

bioRxiv preprint doi: https://doi.org/10.1101/2023.12.17.572059; this version posted December 17, 2023. The copyright holder for this preprint (which was not certified by peer review) is the author/funder, who has granted bioRxiv a license to display the preprint in perpetuity. It is made available under a CC-BY-NC-ND 4.0 International license.



Supplementary Figure 3: Toluidine blue staining does not positively stain mast cells in the ovine mammary gland. (a) Toluidine blue staining in a positive control tissue, a mast cell tumour. (b, c) Sequentially cut sections of FFPE ovine mammary gland tissue. (b) Dual immunohistochemical staining for c-Kit and alpha-SMA. Arrows indicate positive staining for mast cells. (c) Toluidine blue staining. Arrows indicate areas where positive toluidine staining should be. Images representative of 3 biological repeats. All IHC shown with a haematoxylin counterstain. Scale bar = 100 µm (a); 50 µm (b, c).

bioRxiv preprint doi: https://doi.org/10.1101/2023.12.17.572059; this version posted December 17, 2023. The copyright holder for this preprint (which was not certified by peer review) is the author/funder, who has granted bioRxiv a license to display the preprint in perpetuity. It is made available under a CC-BY-NC-ND 4.0 International license.

740 Supplementary Table 1: Full details of sheep used in the study.

Sheep i.d.	Sex	Source	Age	Breed	UK Meteorological Season Died/Euthanised	Neutered Status	Staining
L44	Male	Diagnostic PM	7 weeks	Mule Cross	Spring	Intact	CUBIC (SMA), CUBIC (IBA1/SMA)
L45	Male	Research	3 days	Welsh Mountain	Spring	Intact	CUBIC (SMA), CUBIC (IBA1/SMA)
S84	Male	Research	Mature (2 years +)	Welsh Mountain	Winter	Intact	Ki67/SMA, AR/SMA, ER/SMA, PR/SMA, IBA1/SMA, CD3/CD20, cKit/SMA
S131	Male	Diagnostic PM	6 months	Shetland	Summer	Neutered	Ki67/SMA, AR/SMA, ER/SMA, PR/SMA, IBA1/SMA, CD3/CD20, cKit/SMA
S132	Male	Diagnostic PM	Mature (2 years +)	Unknown	Autumn	Intact	Ki67/SMA, AR/SMA, ER/SMA, PR/SMA, IBA1/SMA, CD3/CD20, cKit/SMA
S133	Male	Diagnostic PM	9 months	Unknown	Winter	Neutered	IBA1/SMA
S154	Male	Diagnostic PM	Mature (2 years +)	Unknown	Spring	Intact	Ki67/SMA, AR/SMA, ER/SMA, PR/SMA, IBA1/SMA, CD3/CD20, cKit/SMA
P20/97	Male	Diagnostic PM	4 months	Mule	Summer	Neutered	Ki67/SMA, AR/SMA, ER/SMA, PR/SMA, IBA1/SMA, CD3/CD20, cKit/SMA
P20/154	Male	Diagnostic PM	Mature (3 years)	Suffolk	Autumn	Intact	Ki67/SMA, IBA1/SMA, cKit/SMA
P21/357	Male	Diagnostic PM	8 months	Cheviot Cross	Autumn	Neutered	Ki67/SMA, AR/SMA, ER/SMA, PR/SMA, IBA1/SMA, CD3/CD20, cKit/SMA
P21/358	Male	Diagnostic PM	8 months	New Zealand Romney	Autumn	Neutered	Ki67/SMA, AR/SMA, ER/SMA, PR/SMA, IBA1/SMA, CD3/CD20, cKit/SMA
P21/366	Male	Diagnostic PM	9 months	Cheviot Cross	Winter	Neutered	Ki67/SMA, AR/SMA, ER/SMA, PR/SMA, IBA1/SMA, CD3/CD20, cKit/SMA
P21/367	Male	Diagnostic PM	10 months	Cheviot Cross	Winter	Neutered	Ki67/SMA, AR/SMA, ER/SMA, PR/SMA, IBA1/SMA, CD3/CD20, cKit/SMA
P21/369	Male	Diagnostic PM	11 months	Cheviot Cross	Winter	Neutered	Ki67/SMA, AR/SMA, ER/SMA, PR/SMA, IBA1/SMA, CD3/CD20
P22/66	Male	Diagnostic PM	14 months	Welsh Mountain	Spring	Intact	Ki67/SMA, AR/SMA, ER/SMA, PR/SMA, IBA1/SMA, CD3/CD20, cKit/SMA
P22/27	Male	Diagnostic PM	8 months	Texel Cross	Winter	Neutered	Ki67/SMA, AR/SMA, ER/SMA, PR/SMA, IBA1/SMA, CD3/CD20, cKit/SMA
P22/233	Male	Diagnostic PM	5 months	Texel Cross	Autumn	Intact	Ki67/SMA, AR/SMA, ER/SMA, PR/SMA, IBA1/SMA, CD3/CD20, cKit/SMA
P23/130	Male	Diagnostic PM	7 weeks	Texel Cross	Spring	Neutered	CUBIC (SMA), CUBIC (IBA1/SMA)
P23/133	Male	Diagnostic PM	Mature (2 years +)	Jacob Cross	Spring	Neutered	Ki67/SMA, AR/SMA, ER/SMA, PR/SMA, IBA1/SMA, CD3/CD20
P16 138	Female	Diagnostic PM	5 months	Texel Cross	Summer	Intact	Ki67/SMA, AR/SMA, ER/SMA, PR/SMA
P18 247	Female	Diagnostic PM	4 months	Beltex	Autumn	Intact	Ki67/SMA, AR/SMA, ER/SMA, PR/SMA
S43	Female	Research	8 months	Welsh Mountain	Winter	Intact	Ki67/SMA, AR/SMA, ER/SMA, PR/SMA
S44	Female	Research	11 months	Welsh Mountain	Winter	Intact	Ki67/SMA, AR/SMA, ER/SMA, PR/SMA
S47	Female	Research	9 months	Welsh Mountain	Winter	Intact	Ki67/SMA, AR/SMA, ER/SMA, PR/SMA
S52	Female	Research	9 months	Welsh Mountain	Spring	Intact	Ki67/SMA, AR/SMA, ER/SMA, PR/SMA
S78	Female	Research	11 months	Welsh Mountain	Autumn	Intact	Ki67/SMA, AR/SMA, ER/SMA, PR/SMA
S141	Female	Research	Mature (2 years +)	Welsh Mountain	Summer	Intact	Ki67/SMA, AR/SMA, ER/SMA, PR/SMA
S142	Female	Research	Mature (2 years +)	Welsh Mountain	Summer	Intact	Ki67/SMA, AR/SMA, ER/SMA, PR/SMA

bioRxiv preprint doi: https://doi.org/10.1101/2023.12.17.572059; this version posted December 17, 2023. The copyright holder for this preprint (which was not certified by peer review) is the author/funder, who has granted bioRxiv a license to display the preprint in perpetuity. It is made available under a CC-BY-NC-ND 4.0 International license.

S143	Female	Research	Mature (2 years +)	Welsh Mountain	Summer	Intact	Ki67/SMA, AR/SMA, ER/SMA, PR/SMA
S144	Female	Research	Mature (2 years +)	Welsh Mountain	Summer	Intact	Ki67/SMA, AR/SMA, ER/SMA, PR/SMA
S145	Female	Research	Mature (2 years +)	Welsh Mountain	Summer	Intact	Ki67/SMA, AR/SMA, ER/SMA, PR/SMA
S146	Female	Research	Mature (2 years +)	Welsh Mountain	Summer	Intact	Ki67/SMA, AR/SMA, ER/SMA, PR/SMA
S147	Female	Research	Mature (2 years +)	Welsh Mountain	Summer	Intact	Ki67/SMA, AR/SMA, ER/SMA, PR/SMA

741

742

bioRxiv preprint doi: https://doi.org/10.1101/2023.12.17.572059; this version posted December 17, 2023. The copyright holder for this preprint (which was not certified by peer review) is the author/funder, who has granted bioRxiv a license to display the preprint in perpetuity. It is made available under a CC-BY-NC-ND 4.0 International license.

743 Supplementary Table 2: Full details of primary and secondary antibodies utilised in

744 immunohistochemical, immunofluorescence and CUBIC staining.

Target	Application (IHC, immunohistochemistry; IF, immunofluorescence; CUBIC, 3D tissue clearing)	Species and Clone (where stated)	Dilution	Manufacturer	Catalogue number
Primary antibodies					
E-cadherin	IF	Mouse monoclonal anti-human [NCH-38]	1:100	Dako/Agilent	M3612
Alpha Smooth muscle actin	Dual colour IHC, CUBIC	Mouse monoclonal anti-human [1A4]	1:500 (dual colour IHC), 1:100 (CUBIC)	Dako/Agilent	M0851
Alpha Smooth muscle actin	Dual colour IHC, IF	Rabbit monoclonal [EPR5368]	1:2000	Abcam	Ab124964
Ki67	Dual colour IHC	Mouse monoclonal anti-human [MIB-1]	1:100	Dako/Agilent	M7240
Androgen Receptor	IF	Rabbit monoclonal [EPR1535(2)]	1:100	Abcam	Ab133273
Oestrogen Receptor α	IF	Rabbit monoclonal [D6R2W]	1:200	Cell Signalling Technology	13258S
Progesterone Receptor A/B	IF	Rabbit monoclonal [D8Q2J]	1:1000	Cell Signalling Technology	8757S
IBA1	Dual colour IHC, CUBIC	Rabbit monoclonal [EPR16588]	1:1200 (dual colour IHC), 1:400 (CUBIC)	Abcam	Ab178846
CD3	Dual colour IHC	Mouse monoclonal [F7.2.38]	1:250	Dako/Agilent	M7254
CD20	Dual colour IHC	Rabbit monoclonal [E7B7T]	1:500	Cell Signalling Technology	48750S
c-Kit	Dual colour IHC	Rabbit monoclonal [D3W6Y]	1:100	Cell Signalling Technology	37805S
Secondary antibodies					
Mouse IgG, Alexa Fluor Plus 488	IF, CUBIC	Goat	1:500	Thermo Fisher Scientific	A32723
Rabbit IgG, Alexa Fluor Plus 647	IF, CUBIC	Goat	1:500	Thermo Fisher Scientific	A32733

745